

SOLAR-LIKE OSCILLATIONS IN THE G2 SUBGIANT β HYDRI FROM DUAL-SITE OBSERVATIONS

TIMOTHY R. BEDDING,¹ HANS KJELDSSEN,² TORBEN ARENTOFT,² FRANCOIS BOUCHY,^{3,4} JACOB BRANDBYGE,²
BRENDON J. BREWER,¹ R. PAUL BUTLER,⁵ JØRGEN CHRISTENSEN-DALSGAARD,² THOMAS DALL,⁶ SØREN FRANDSEN,²
CHRISTOFFER KAROFF,² LÁSZLÓ L. KISS,¹ MARIO J.P.F.G. MONTEIRO,⁷ FRANK P. PIJPERS,⁸ TERESA C. TEIXEIRA,⁷
C. G. TINNEY,⁹ IVAN K. BALDRY,^{9,10} FABIEN CARRIER,^{3,11} AND SIMON J. O'TOOLE^{1,9}

to appear in ApJ

ABSTRACT

We have observed oscillations in the nearby G2 subgiant star β Hyi using high-precision velocity observations obtained over more than a week with the HARPS and UCLES spectrographs. The oscillation frequencies show a regular comb structure, as expected for solar-like oscillations, but with several $l = 1$ modes being strongly affected by avoided crossings. The data, combined with those we obtained five years earlier, allow us to identify 28 oscillation modes. By scaling the large frequency separation from the Sun, we measure the mean density of β Hyi to an accuracy of 0.6%. The amplitudes of the oscillations are about 2.5 times solar and the mode lifetime is 2.3 d. A detailed comparison of the mixed $l = 1$ modes with theoretical models should allow a precise estimate of the age of the star.

Subject headings: stars: individual (β Hyi) — stars: oscillations

1. INTRODUCTION

There has been tremendous recent progress in observing solar-like oscillations in main-sequence and subgiant stars. In a few short years we have moved from ambiguous detections to firm measurements (see Bedding & Kjeldsen 2006 for a recent summary). Most of the results have come from high-precision Doppler measurements using spectrographs such as CORALIE, HARPS, UCLES and UVES.

The star β Hydri (HR 98, HD 2151, HIP 2021) is a bright southern G2 subgiant ($V = 2.80$) that is an excellent target for asteroseismology. Early unsuccessful attempts to measure oscillations were made by Frandsen (1987) and Edmonds & Cram (1995). Five years ago we

reported oscillations in this star from velocity measurements made with UCLES (Bedding et al. 2001) and confirmed with CORALIE (Carrier et al. 2001). Those observations implied a large frequency separation of 56–58 μHz but did not allow the unambiguous identification of individual modes. Meanwhile, theoretical models for β Hyi have been published by Fernandes & Monteiro (2003) and Di Mauro et al. (2003), with both studies indicating the occurrence of avoided crossings for modes with $l = 1$ (see §4). This goes a long way toward explaining the earlier difficulty in mode identification.

Here we report new observations of β Hyi using HARPS and UCLES in a dual-site campaign. We confirm the earlier detection of oscillations and are able to identify nearly 30 modes, including some which show the clear effect of avoided crossings. We also measure the amplitudes of the oscillations and the mode lifetimes, and use the large separation to infer the mean stellar density.

2. VELOCITY OBSERVATIONS AND POWER SPECTRA

We observed β Hyi in 2005 September from two sites. At the European Southern Observatory on La Silla in Chile we used the HARPS spectrograph (High Accuracy Radial velocity Planet Searcher) with the 3.6-m telescope¹². A thorium emission lamp was used to calibrate the velocities, which were extracted using the HARPS pipeline (Rupprecht et al. 2004). At Siding Spring Observatory in Australia we used UCLES (University College London Échelle Spectrograph) with the 3.9-m Anglo-Australian Telescope (AAT). An iodine absorption cell was used to provide a stable wavelength reference, with the same setup that we have previously used with this spectrograph for β Hyi (Bedding et al. 2001) and other stars.

With HARPS we obtained 2766 spectra of β Hyi, with a dead time between exposures of 31 s and exposure times of 40 or 50 s, depending on the conditions. With UCLES

¹² Based on observations collected at the European Southern Observatory, La Silla, Chile (ESO Programme 75.D-0760(A)).

¹ School of Physics A28, University of Sydney, NSW 2006, Australia; bedding@physics.usyd.edu.au; brewer@physics.usyd.edu.au; laszlo@physics.usyd.edu.au

² Danish AsteroSeismology Centre (DASC), Department of Physics and Astronomy, University of Aarhus, DK-8000 Aarhus C, Denmark; hans@phys.au.dk, toar@phys.au.dk, jacob@phys.au.dk, srf@phys.au.dk, jcd@phys.au.dk, karoff@phys.au.dk

³ Observatoire de Genève, Ch. des Maillettes 51, CH-1290 Sauverny, Switzerland; francois.bouchy@obs.unige.ch

⁴ Laboratoire d'Astrophysique de Marseille, Traverse du Siphon, BP 8, 13376 Marseille Cedex 12, France

⁵ Carnegie Institution of Washington, Department of Terrestrial Magnetism, 5241 Broad Branch Road NW, Washington, DC 20015-1305; paul@dtm.ciw.edu

⁶ European Southern Observatory, Casilla 19001, Santiago 19, Chile; tdall@eso.org

⁷ Faculdade de Ciências and Centro de Centro de Astrofísica da Universidade do Porto, Rua das Estrelas, 4150-762 Porto, Portugal; mjm@astro.up.pt

⁸ Blackett Laboratory, Imperial College London, South Kensington, London SW7 2BW, UK; f.pijpers@imperial.ac.uk

⁹ Anglo-Australian Observatory, P.O. Box 296, Epping, NSW 1710, Australia; cgt@aaoepp.aao.gov.au; otoole@aaoepp.aao.gov.au

¹⁰ Astrophysics Research Institute, Liverpool John Moores University, Egerton Wharf, Birkenhead, CH41 1LD, UK; ikb@astro.livjm.ac.uk

¹¹ Instituut voor Sterrenkunde, Katholieke Universiteit Leuven, Celestijnenlaan 200 B, 3001 Leuven, Belgium; fabien@ster.kuleuven.be

we obtained 1191 spectra, with a dead time between exposures of 70s and exposure times in the range 60–180s, such that the median sampling time was 187s (implying a Nyquist frequency of about 2.7 mHz).

The resulting velocities are shown in Fig. 1. As can be seen, the weather was very good in Chile but only moderately good in Australia (we were allocated 7 nights with HARPS and 12 with UCLES). The seeing was also much better in Chile. Most of the scatter in the velocities is due to oscillations, but there are also slow variations and night-to-night variations in both series that we ascribe to instrumental effects. Figure 2 shows close-up views during the four brief periods in which both telescopes were observing simultaneously. Note that the velocity offsets between the two data sets were adjusted separately in each segment, to compensate for differential drifts between the two instruments. After this was done, we see excellent agreement between the two data sets.

Figure 3 shows the power spectra of the two time series. The signal from stellar oscillations appears as the broad excess of power centered at 1 mHz. As usual, we have used the measurement uncertainties, σ_i , as weights in calculating these power spectra (according to $w_i = 1/\sigma_i^2$). In the case of HARPS, these uncertainties were provided by the data processing pipeline. For UCLES, they were estimated from the scatter in the residuals during the measurement, as described by Butler et al. (1996).

The peak in the HARPS power spectrum at 3070 μHz (and another at twice this frequency, not shown here) is due to a periodic error in the guiding system, as previously noted by Carrier & Eggenberger (2006) and Bazot et al. (2007). Fortunately, this signal is restricted to a fairly narrow band of frequencies that lies well above the oscillations of β Hyi, so it does not compromise the data.

In analysing the data, we have followed basically the same method that we used for α Cen A (Butler et al. 2004; Bedding et al. 2004), α Cen B (Kjeldsen et al. 2005) and ν Ind (Bedding et al. 2006). Our initial goal was to adjust the weights in order to minimize the noise level in the Fourier spectrum (§ 2.1). Having done this, we then made further adjustments with the aim of reducing the sidelobes in the spectral window (§ 2.2).

2.1. Optimizing for Signal-to-Noise

We have chosen to measure the noise in the amplitude spectrum, σ_{amp} , in two frequency bands on either side of the oscillation signal: 230–420 μHz and 1800–2100 μHz , as indicated by the dotted lines in Fig. 3. We averaged these using the geometric mean (since instrumental noise varies as an inverse power of frequency). Using this criterion the power spectra in Fig. 3 have noise levels (in amplitude) of 6.1 cm s^{-1} for HARPS and 11 cm s^{-1} for UCLES. These values imply a noise per minute of observing time, before any further optimization, of 1.9 m s^{-1} for HARPS and 3.7 m s^{-1} for UCLES. The difference is due to a combination of factors, primarily the observing duty cycle and sky conditions.

The first step in optimizing the weights was to modify some of them to account for a small fraction of bad data points, in the same way that we have done for other stars (see Butler et al. 2004 for details). In brief, this involved (i) cleaning from the time series all power at low frequencies (below 200 μHz), as well as all power from oscillations

(500–1400 μHz); and (ii) searching these residuals for points that deviated from zero by more than would be expected from their uncertainties. We found that 78 data points from HARPS (2.8%) and 25 from UCLES (2.1%) needed to be significantly down-weighted.

The next step in reducing the noise involved ensuring that the uncertainties we are using to calculate the weights reflect the actual scatter in the data. By this, we mean that the estimates of σ_i should be consistent with the noise level determined from the amplitude spectrum, which means they should satisfy equation (3) of Butler et al. (2004):

$$\sigma_{\text{amp}}^2 \sum_{i=1}^N \sigma_i^{-2} = \pi. \quad (1)$$

We checked this on a night-by-night basis for both instruments, measuring σ_{amp} in the way described above. The results showed that the uncertainties σ_i for HARPS should be multiplied by a factor that ranged from 2.6 to 4.3, while for UCLES the factor ranged from 0.57 to 0.73. The variations in this factor from night to night presumably reflect changes in the instrumental stability. Note that the factor for UCLES can be compared with the value of 0.87 that we estimated for α Cen A (Butler et al. 2004), which was however determined from measuring the noise at much higher frequencies and for the run as a whole. For HARPS, the large discrepancy between the uncertainties estimated by the pipeline and those required to explain the scatter in the data has been noted previously, at levels consistent with our results (Bouchy et al. 2005; Carrier & Eggenberger 2006; Bazot et al. 2007).

With the velocity uncertainties corrected in this way, we found that HARPS gave a mean precision per spectrum on β Hyi of about 1.4 m s^{-1} and UCLES gave 1.7 m s^{-1} (with a spread during the run of about 20%). However, HARPS was able to record spectra at about twice the rate of UCLES, thanks to the better atmospheric conditions (which allowed shorter exposure times) and the faster CCD readout.

The power spectrum of the combined time series is shown in Fig. 4 and the noise level is 4.2 cm s^{-1} in amplitude. We refer to this as the noise-optimized power spectrum. Note that the time series has been high-pass filtered in order to account for the varying offsets between the two data sets and to prevent power from slow variations from leaking into the oscillation signal.

2.2. Optimizing for sidelobes

The inset in Fig. 4 shows the spectral window (the response to a single pure sinusoid) and we see sidelobes at \pm one cycle per day (11.6 μHz) that are moderately strong (25% in power). A close-up is shown in Fig. 5a. These sidelobes occur despite there being relatively few gaps in the observing window because of the higher rate of data collection with HARPS as compared to UCLES.

As for our analysis of α Cen A and B, we have also generated a power spectrum in which the weights were adjusted on a night-by-night basis in order to minimize the sidelobes. This involved giving greater weight to the UCLES data (multiplying the weights by a factor that was typically about 10) and resulted in a spectral window with sidelobes reduced to only 4.1% in power (see

Fig. 5b). The trade-off is an increase in the noise level, which rose to 6.2 cm s^{-1} in amplitude.

Finally, we also calculated a power spectrum based on the best five nights from both sites ($\text{JD} - 2453600 = 17.5$ to 22.5 ; see Fig. 1). In this case, the weights given to the five nights of UCLES data were increased by a single factor of 7.2 to lower the sidelobes, whose resulting height was 15.7% in power (see Fig. 5c). The noise in this amplitude spectrum was 6.2 cm s^{-1} . This power spectrum has similar noise to the sidelobe-optimized version and higher sidelobes, but it has the important property of covering a shorter period of time. We expect the modes in β Hyi to have lifetimes of a few days, and so the best signal-to-noise will be achieved in a time series that is not too much longer than this. Once the observing time greatly exceeds the mode lifetime, the oscillation modes in the power spectrum become resolved (eventually splitting into a cluster of peaks under a Lorentzian envelope) and the signal-to-noise of the peaks no longer improves with increased observing time.

3. RE-ANALYSIS OF THE 2000 OBSERVATIONS

To allow us to detect as many oscillation modes as possible in β Hyi, our analysis included our 2000 June observations. These data consist of five nights with UCLES (Bedding et al. 2001) and 14 nights with the CORALIE spectrograph in Chile (Carrier et al. 2001), with the latter being affected by bad weather. The two time series are shown in Fig. 6.

The UCLES échelle spectra have been completely re-processed, using new packages for the raw reduction and velocity extraction, resulting in an improvement in precision at high frequencies of 13%. We have not re-analyzed the CORALIE spectra and so these velocities are the same as already published (Carrier et al. 2001).

We subjected both 2000 velocity time series to the same analysis that is described above. The combined noise-optimized power spectrum is shown in Fig. 7. The noise averaged over our defined frequency ranges is 5.9 cm s^{-1} in amplitude. The spectral window is shown in the inset and also in close-up in Fig. 5d. The sidelobe-optimized version of these data has a noise level of 8.0 cm s^{-1} and its spectral window is shown in Fig. 5e.

4. OSCILLATION FREQUENCIES

Mode frequencies for low-degree p-mode oscillations in main-sequence stars are well approximated by a regular series of peaks, with frequencies given by the following asymptotic relation:

$$\nu_{n,l} = \Delta\nu(n + \frac{1}{2}l + \epsilon) - l(l+1)D_0. \quad (2)$$

Here n (the radial order) and l (the angular degree) are integers, $\Delta\nu$ (the large separation) depends on the sound travel time across the whole star, D_0 is sensitive to the sound speed near the core and ϵ is sensitive to the surface layers. See Christensen-Dalsgaard (2004) for a recent review of the theory of solar-like oscillations.

A subgiant such as β Hyi is expected to show substantial deviations from the regular comb-like structure described by equation (2). This is because some mode frequencies, particularly those with $l = 1$, are shifted by avoided crossings with gravity modes in the stellar core (also called ‘mode bumping’; see Aizenman et al.

1977). These shifted modes are known as ‘mixed modes’ because they have p-mode character near the surface but g-mode character in the deep interior. Theoretical models of β Hyi indeed predict these mixed modes (Di Mauro et al. 2003; Fernandes & Monteiro 2003), and we must keep this in mind when attempting to identify oscillation modes in the power spectrum. The mixed modes are rich in information because they probe the stellar core and are very sensitive to age, but they complicate greatly the task of mode identification.

We have extracted oscillation frequencies from the time series using the standard procedure of iterative sine-wave fitting. Each step of the iteration involves finding the strongest peak in the power spectrum and subtracting the corresponding sinusoid from the time series. At each step, the frequencies, amplitudes and phases of all extracted peaks were adjusted simultaneously to give the best fit. In analysing these frequencies, the first step was to determine the large separation. We did this by examining the pair-wise differences between frequencies extracted from the noise-optimized 2005 power spectrum. We included all peaks with $S/N \geq 4$ (46 peaks) and found the strongest signals at 29.1 and $57.2 \mu\text{Hz}$. We identify these as corresponding to $\Delta\nu/2$ and $\Delta\nu$, respectively, consistent with the values published from the 2000 observations (Bedding et al. 2001; Carrier et al. 2001).

With the large separation established, we next sought to identify modes in the échelle diagram. Figure 8 shows only the very strongest peaks in the 2005 data ($S/N \geq 7$). Different symbols are used to show the three weighting schemes and the symbol size is proportional to the S/N . We can immediately identify the ridges corresponding to modes with $l = 0$ and $l = 2$, both of which are expected to be unaffected by avoided crossings. The positions of these two ridges, marked by the vertical solid lines, allow us to calculate the expected positions of modes with $l = 1$ and $l = 3$, based on the asymptotic relation (equation 2). These are shown by dashed lines in the figure. A few of the peaks in that region of the diagram fall close to the $l = 1$ line, but most do not. We are clearly seeing several mixed modes in β Hyi.

Deciding which peaks correspond to genuine modes is always a subjective process. There is a trade-off between the desire to find as many oscillation modes as possible and the risk of identifying noise peaks as genuine. There is also the danger, especially for the weaker peaks, that the sidelobe will be stronger than the real peak because of interference with the noise, leading to an aliasing error of $\pm 11.6 \mu\text{Hz}$. And for an evolved star like β Hyi, we have the added complication of mixed modes.

In the case of β Hyi, we have the advantage of two independent data sets taken five years apart. The 2005 data have extremely low noise and a very good window function. The 2000 data have higher noise and more gaps, but the sidelobe-optimized weighting still gives a good spectral window. In Fig. 9 we show all peaks extracted from the time series that have $S/N \geq 4$. At this level, very few of the peaks should be due to noise. We again used different symbols to identify the different weighting schemes, as shown in the figure legend.

The circles in Fig. 9 show the final frequencies, which are listed in Table 1. Given the effects of noise and finite mode lifetime, we do not expect perfect agreement between different measurements of the same mode. In cases

where a peak was detected in more than one weighting scheme, we have averaged the frequency measurements. In those cases, the S/N in the table refers to the maximum among the contributors.

The 28 frequencies above the line are those for which we are confident of the identification. These are also shown in Fig. 11, where we see a pattern of mixed modes that is strikingly similar to that calculated from models by Di Mauro et al. (2003). Note that the n values in Table 1 were determined on the assumption that ϵ falls in the range $1 \leq \epsilon \leq 2$, as it does in the Sun. The 29 frequencies below the line in the table will include some genuine modes, some sidelobes that need to be shifted by $\pm 11.6 \mu\text{Hz}$, and some noise peaks. We list them here for completeness, to allow comparison with oscillation models of β Hyi.

The uncertainties in the mode frequencies are shown in parentheses in Table 1. These depend on the S/N ratio of the peak and were calculated from the simulations described in §6, assuming the value of the mode lifetime derived in that section. Of course, these frequency uncertainties are based on the assumption that the corresponding peaks in the power spectrum are caused by a genuine oscillation modes and are not noise peaks or aliases.

We have looked for a systematic offset between mode frequencies of β Hyi from the 2005 and 2000 observations. Such an offset could indicate variations during a stellar activity cycle, as has tentatively been suggested for α Cen A (Fletcher et al. 2006). We find that the 2005 frequencies are lower than the 2000 frequencies by an average amount of $0.1 \pm 0.4 \mu\text{Hz}$, which is consistent with zero. Finally, of the two mode identifications suggested by Bedding et al. (2001), we can now identify solution B as being closest to the correct one.

4.1. Frequencies from a Bayesian treatment

We have recently described an alternative approach to extracting frequencies from a time series, which we applied to the star ν Ind, using Bayesian methods rather than Fourier analysis (Bedding et al. 2006; Brewer et al. 2007). We have applied a similar technique to β Hyi, using the noise-optimized 2005 time series. This analysis differed in one important respect from that on ν Ind: we did not make any assumptions about the distribution of frequencies.

The results are shown in Fig. 10, where the diamonds are the same as in Fig. 9 and the circles are the most probable frequencies found by the Bayesian method. In most cases there is excellent agreement between the two analyses. There is a peak at $1262.20 \mu\text{Hz}$, which lies exactly on the $l = 1$ ridge, that only appears in Bayesian analysis. In fact, this peak was found with $S/N = 3.0$ by the traditional method and we have shown it as a genuine mode in Table 1 and Fig. 11.

4.2. Frequency separations and inferred stellar parameters

The large separation $\Delta\nu$ is a function of the mode degree, l , and also varies with frequency. We have determined it for both $l = 0$ and 2 by fitting to the modes identified in Table 1 and shown in Fig. 11. The values at 1 mHz are given in Table 2. We also give the small

separation $\delta\nu_{02}$ between $l = 0$ and 2 , and the implied values for the parameters D_0 and ϵ .

A detailed comparison of the oscillation frequencies of β Hyi with theoretical models is beyond the scope of this paper. Here, we restrict ourselves to using the large separation to estimate the mean density of the star. To a good approximation, the large separation is proportional to the square root of the mean stellar density:

$$\frac{\Delta\nu}{\Delta\nu_{\odot}} = \sqrt{\frac{\bar{\rho}}{\bar{\rho}_{\odot}}}. \quad (3)$$

However, it is well-known that models – even for the Sun – are not yet good enough to reproduce the observed frequencies due to improper modelling of the surface layers (Christensen-Dalsgaard et al. 1988). There is a systematic offset between observed and computed frequencies that increases with frequency, and hence leads to an incorrect prediction for the large separation.

We have examined this surface effect in detail for models of the Sun and β Hyi (Kjeldsen & Bedding, in prep.) and found that the correction term scales in such a way that, provided that $\Delta\nu$ is measured at the peak of the oscillation envelope, equation (3) remains an excellent approximation. We have therefore used equation (3) to estimate the mean density of β Hyi from our measurement of $\Delta\nu_0$. We used a value of $134.81 \pm 0.09 \mu\text{Hz}$ for the large separation of radial modes in the Sun, which we obtained by fitting in the range $n = 17\text{--}25$ to the frequencies measured by Lazrek et al. (1997) using the GOLF instrument on the SOHO spacecraft. The resulting mean density for β Hyi has an uncertainty of only 0.6% and is given in Table 2.

5. OSCILLATION AMPLITUDES

The amplitudes of individual modes are affected by the stochastic nature of the excitation and damping. To measure the oscillation amplitude of β Hyi in a way that is independent of these effects, we have followed the method introduced by Kjeldsen et al. (2005). In brief, this involves the following steps: (i) smoothing the power spectrum heavily to produce a single hump of excess power that is insensitive to the fact that the oscillation spectrum has discrete peaks; (ii) converting to power density by multiplying by the effective length of the observing run (which we calculated from the area under the spectral window in power); (iii) fitting and subtracting the background noise; and (vi) multiplying by $\Delta\nu/3.0$ and taking the square root, in order to convert to amplitude per oscillation mode. For more details, see Kjeldsen et al. (2005).

The result is shown in Fig. 12 for both the 2005 and 2000 observations. The difference between the two runs, which were made five years apart, is not surprising when we recall that the solar amplitude, when measured in the same way, shows similar variations from week to week. The peak amplitude per mode in β Hyi is $40\text{--}50 \text{ cm s}^{-1}$, which occurs at a frequency of $\nu_{\text{max}} = 1.0 \text{ mHz}$. This value of ν_{max} is consistent with that expected from scaling the acoustic cutoff frequency of the Sun (Brown et al. 1991; Kjeldsen & Bedding 1995). The observed peak amplitude is about 2.5 times the solar value, when the latter is measured using stellar techniques (Kjeldsen et al., in prep.). Given the uncertainties, this is consistent with

the values of 3.2 expected from the L/M scaling proposed by Kjeldsen & Bedding (1995) and also with 2.2 from the $(L/M)^{0.7}$ scaling proposed by Samadi et al. (2005).

6. MODE LIFETIMES

We can estimate the lifetime of solar-like oscillations from the scatter of the observed frequencies about the ridges in the échelle diagram (see Kjeldsen et al. 2005). For β Hyi we used only the $l = 0$ and 2 modes, since these are apparently unaffected by avoided crossing. In addition, we examined the differences between the 2000 and 2005 data sets for those modes that were detected in both (assuming that any differences due to a stellar activity cycle are negligible; see §4). We found the mean scatter per mode to be $1.25 \pm 0.15 \mu\text{Hz}$. Following the method described by Kjeldsen et al. (2005), this frequency scatter was calibrated using simulations having a range of mode lifetimes and with the observed S/N, window function and weights. We assumed that any rotational splitting could be neglected, which is certainly reasonable given the very low measured rotational velocity of the star of $2\text{--}5 \text{ km s}^{-1}$ (Dravins & Nordlund 1990; Reiners & Schmitt 2003; Setiawan et al. 2004).

We carried out the simulations for ten different values of the mode lifetime and the results are shown in Figure 13, where each point represents the mean of 300 simulations. The solid curve represents a fit to these points and the two dotted curves on either side reflect the $1\text{-}\sigma$ variations in the simulations. The horizontal dashed line shows the observed scatter in the frequencies, from which we can read off a value for the mode lifetime of $2.18^{+0.77}_{-0.60}$ d.

As a check, we also used a new and completely different method to estimate the mode lifetime. This involved examining the region of excess power in the Fourier spectrum and measuring the ratio between the mean in the power spectrum and the square of the mean amplitude. This ratio, $R = \langle A^2 \rangle / \langle A \rangle^2$, measures the ‘peakiness’ of the power spectrum. For purely Gaussian noise, R will have a value of $4/\pi = 1.27$ (see equation (A2) of Kjeldsen & Bedding 1995), while for a spectrum composed of many strong narrow peaks it will have a much higher value. For example, the observed value of R in the noise-optimized spectrum from 2005 is 1.42 (measured in the range $700\text{--}1300 \mu\text{Hz}$). Note that the ratio of power-to-squared-amplitude is only a sensitive indicator of mode lifetime in the case where the noise level in the spectrum is very low, which is true for our 2005 observations of β Hyi.

We have again calibrated the observed values of R by comparing with simulations with a range of mode lifetimes. The only additional information that we required, beyond repeating the assumption of negligible rotation, was the number of oscillation modes in the spectrum. This is easily calculated from the large separation, provided we assume that there is exactly one mode for each

pair of l and n . For extremely evolved stars in which the spectrum of g-modes is very dense, we would expect more than one mixed mode per order, but for β Hyi this does not appear to be the case (Di Mauro et al. 2003; Fernandes & Monteiro 2003). It is therefore reasonable to assume that, despite the presence of mixed modes, there is still on average only one mode per order for each value of the degree l .

We again carried out the simulations for ten different values of the mode lifetime. The results for the noise-optimized spectrum from 2005 are shown in Figure 14, where each point represents the mean of 300 simulations. The solid curve represents a fit to these points and the two dotted curves on either side reflect the $1\text{-}\sigma$ variations in the simulations. The horizontal dashed line shows the observed value of R , which allows us to determine the mode lifetime. We did the same thing for the other two weighting schemes for the 2005 data (sidelobe-optimized and best five nights). The mean of the three schemes gave a mode lifetime of $2.57^{+1.37}_{-0.82}$ d.

These two estimates are independent in the sense that they rely on two different properties of the power spectrum. The first measures the positions of the peaks and the second measures their amplitudes. We are therefore justified in combining the two estimates for the mode lifetime, and the final value is listed in Table 2. This value, combined with the amplitudes estimated in §5, should allow a comparison with theoretical models of the excitation of solar-like oscillations (Samadi et al. 2007; Houdek 2006).

7. CONCLUSIONS

We have presented dual-site velocity observations of β Hyi that confirm the presence of solar-like oscillations. These data, combined with those we obtained in 2000, allowed us to identify 28 oscillation modes. The large frequency separation allowed us to infer a very precise value for the mean density of β Hyi. We also measured the amplitudes and lifetimes of the oscillations. Finally, the frequencies show the clear signature of mixed $l = 1$ modes which, after comparison with models of this star, should allow a sensitive measure of its age.

We would be happy to make the data presented in this paper available on request.

We thank Geoff Marcy for useful advice and enthusiastic support and Dennis Stello for comments on the manuscript. This work was supported financially by the Australian Research Council, the Swiss National Science Foundation, the Portuguese FCT and POCI2010 (POCI/CTE-AST/57610/2004) with funds from the European programme FEDER and the Danish Natural Science Research Council. We further acknowledge support by NSF grant AST-9988087 (RPB) and by SUN Microsystems.

REFERENCES

- Aizenman, M., Smeyers, P., & Weigert, A., 1977, *A&A*, 58, 41.
 Bazot, M., Bouchy, F., Kjeldsen, H., Charpinet, S., Laymand, M., & Vauclair, S., 2007, *A&A*. submitted.
 Bedding, T. R., Butler, R. P., Carrier, F., Bouchy, F., Brewer, B. J., Eggenberger, P., Grundahl, F., Kjeldsen, H., McCarthy, C., Bjorn Nielsen, T., Retter, A., & Tinney, C. G., 2006, *ApJ*, 647, 558.

- Bedding, T. R., Butler, R. P., Kjeldsen, H., Baldry, I. K., O'Toole, S. J., Tinney, C. G., Marcy, G. W., Kienzle, F., & Carrier, F., 2001, *ApJ*, 549, L105.
- Bedding, T. R., & Kjeldsen, H., 2006, In Fletcher, K., editor, *Beyond the Spherical Sun: a new era in helio- and asteroseismology*, *Proc. SOHO 18/GONG 2006/HelAS I*, SP-624, page 25. astro-ph/0609770.
- Bedding, T. R., Kjeldsen, H., Butler, R. P., McCarthy, C., Marcy, G. W., O'Toole, S. J., Tinney, C. G., & Wright, J. T., 2004, *ApJ*, 614, 380.
- Bouchy, F., Bazot, M., Santos, N. C., Vauclair, S., & Sosnowska, D., 2005, *A&A*, 440, 609.
- Brewer, B. J., Bedding, T. R., Kjeldsen, H., & Stello, D., 2007, *ApJ*, 654, 551.
- Brown, T. M., Gilliland, R. L., Noyes, R. W., & Ramsey, L. W., 1991, *ApJ*, 368, 599.
- Butler, R. P., Bedding, T. R., Kjeldsen, H., McCarthy, C., O'Toole, S. J., Tinney, C. G., Marcy, G. W., & Wright, J. T., 2004, *ApJ*, 600, L75.
- Butler, R. P., Marcy, G. W., Williams, E., McCarthy, C., Dosanji, P., & Vogt, S. S., 1996, *PASP*, 108, 500.
- Carrier, F., Bouchy, F., Kienzle, F., Bedding, T. R., Kjeldsen, H., Butler, R. P., Baldry, I. K., O'Toole, S. J., Tinney, C. G., & Marcy, G. W., 2001, *A&A*, 378, 142.
- Carrier, F., & Eggenberger, P., 2006, *A&A*, 450, 695.
- Christensen-Dalsgaard, J., 2004, *Sol. Phys.*, 220, 137.
- Christensen-Dalsgaard, J., Dappen, W., & Lebreton, Y., 1988, *Nat*, 336, 634.
- Di Mauro, M. P., Christensen-Dalsgaard, J., & Paternò, L., 2003, *Ap&SS*, 284, 229.
- Dravins, D., & Nordlund, Å., 1990, *A&A*, 228, 203.
- Edmonds, P. D., & Cram, L. E., 1995, *MNRAS*, 276, 1295.
- Fernandes, J., & Monteiro, M. J. P. F. G., 2003, *A&A*, 399, 243.
- Fletcher, S. T., Chaplin, W. J., Elsworth, Y., Schou, J., & Buzasi, D., 2006, *MNRAS*, 371, 935.
- Frandsen, S., 1987, *A&A*, 181, 289.
- Houdek, G., 2006, In Fletcher, K., editor, *Beyond the Spherical Sun: a new era in helio- and asteroseismology*, *Proc. SOHO 18/GONG 2006/HelAS I*, SP-624, page 28. astro-ph/0612024.
- Kjeldsen, H., & Bedding, T. R., 1995, *A&A*, 293, 87.
- Kjeldsen, H., Bedding, T. R., Butler, R. P., Christensen-Dalsgaard, J., Kiss, L. L., McCarthy, C., Marcy, G. W., Tinney, C. G., & Wright, J. T., 2005, *ApJ*, 635, 1281.
- Lazrek, M., Baudin, F., Bertello, L., Boumier, P., Charra, J., Fierry-Fraillon, D., Fossat, E., Gabriel, A. H., García, R. A., Gelly, B., Gouiffes, C., Grec, G., Palle, P. L., Perez Hernandez, F., Regulo, C., Renaud, C., Robillot, J.-M., Roca Cortes, T., Turck-Chieze, S., & Ulrich, R. K., 1997, *Sol. Phys.*, 175, 227.
- Reiners, A., & Schmitt, J. H. M. M., 2003, *A&A*, 398, 647.
- Rupprecht, G., Pepe, F., Mayor, M., et al., 2004, In Moorwood, A. F. M., & Masanori, I., editors, *Ground-based Instrumentation for Astronomy*, volume 5492 of *Proc. SPIE*, page 148.
- Samadi, R., Georgobiani, D., Trampedach, R., Goupil, M. J., Stein, R. F., & Nordlund, A., 2007, *A&A*, 463, 297.
- Samadi, R., Goupil, M.-J., Alecian, E., Baudin, F., Georgobiani, D., Trampedach, R., Stein, R., & Nordlund, Å., 2005, *JA&A*, 26, 171.
- Setiawan, J., Pasquini, L., da Silva, L., Hatzes, A. P., von der Lühe, O., Girardi, L., de Medeiros, J. R., & Guenther, E., 2004, *A&A*, 421, 241.

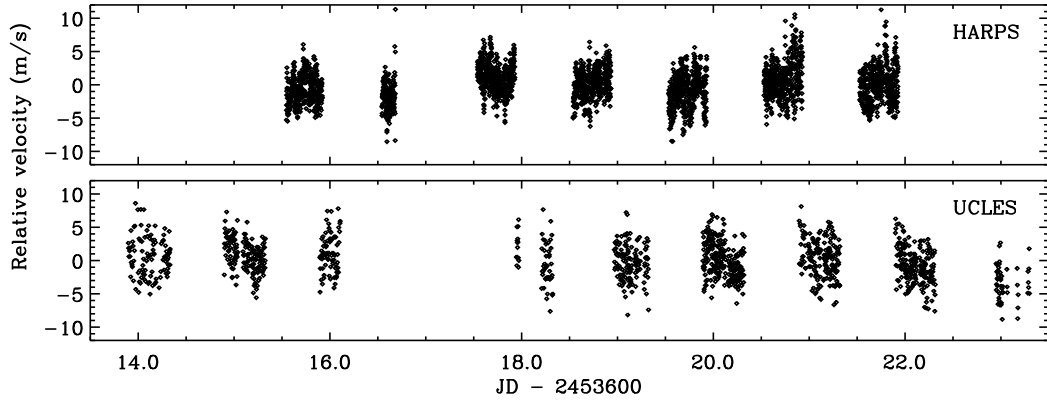


FIG. 1.— Time series of velocity measurements of β Hyi obtained from 2005 August 31 to September 9.

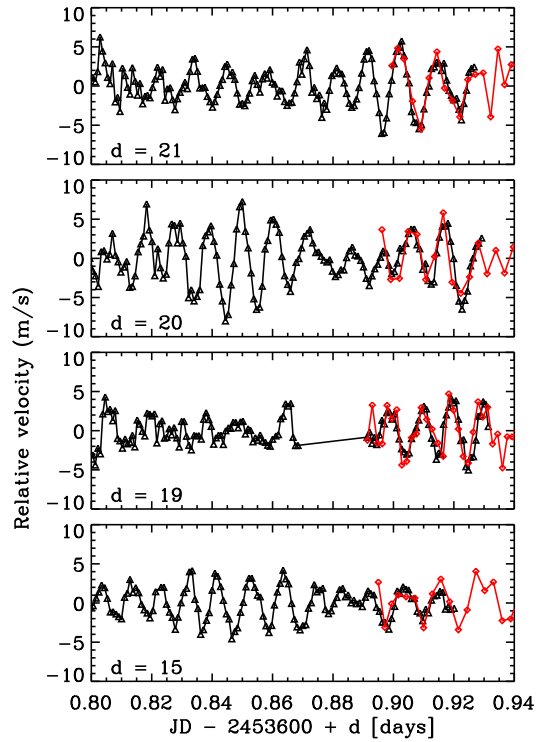


FIG. 2.— Close-ups of the time series in Fig. 1 for the four segments during which both telescopes were observing simultaneously. Black triangles are from HARPS and red diamonds are from UCLES.

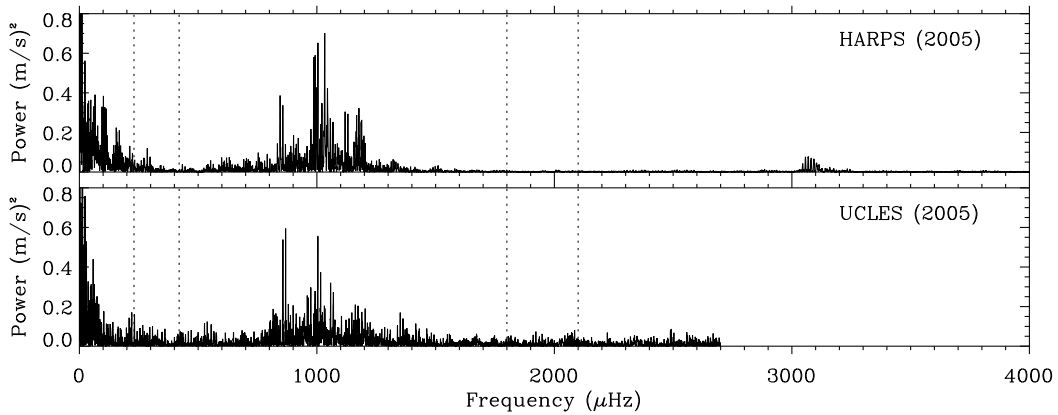


FIG. 3.— Power spectra of β Hyi from the two instruments, based on the data as it emerged from the pipeline (using the uncertainties as weights). The pairs of dotted lines mark the two regions that were used to measure the noise level.

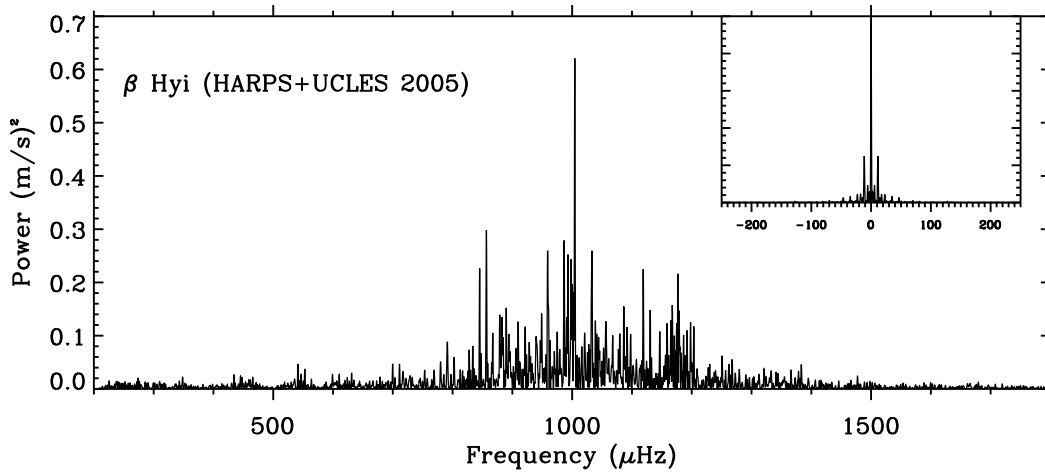


FIG. 4.— Power spectrum of β Hyi after combining the data to optimize the signal-to-noise. The inset shows the spectral window.

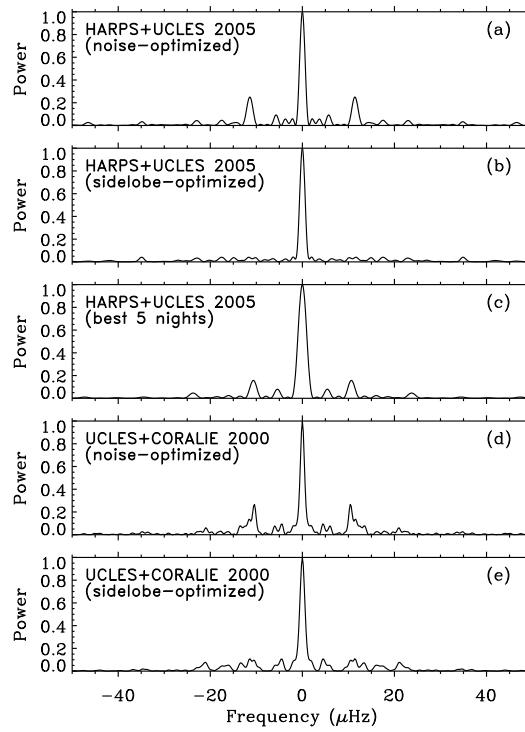


FIG. 5.— Spectral windows for the 2005 and 2000 data, using different weighting schemes (see text).

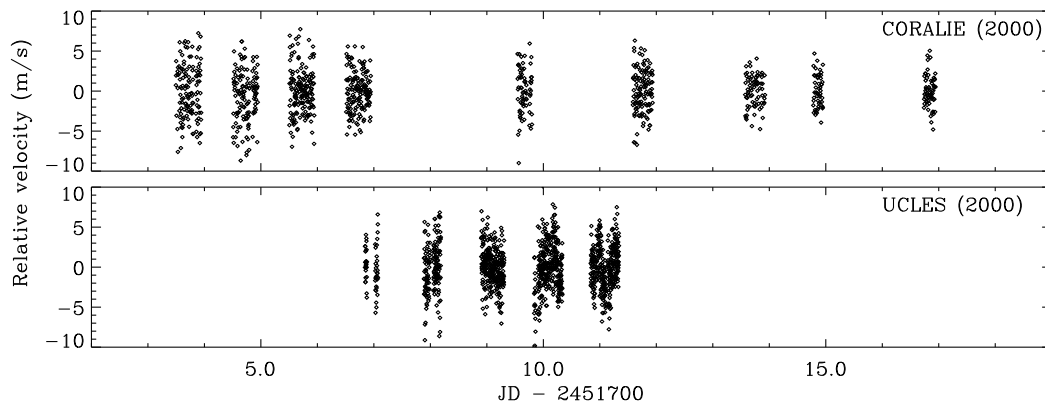


FIG. 6.— Time series of velocity measurements of β Hyi made in 2000 June with UCLES and CORALIE.

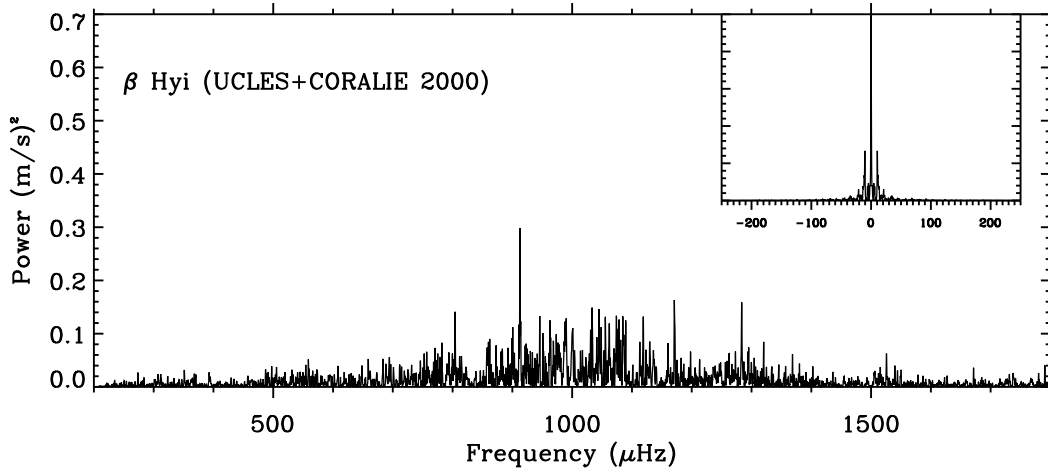


FIG. 7.— Power spectrum of β Hyi from the 2000 observations with UCLES and CORALIE.

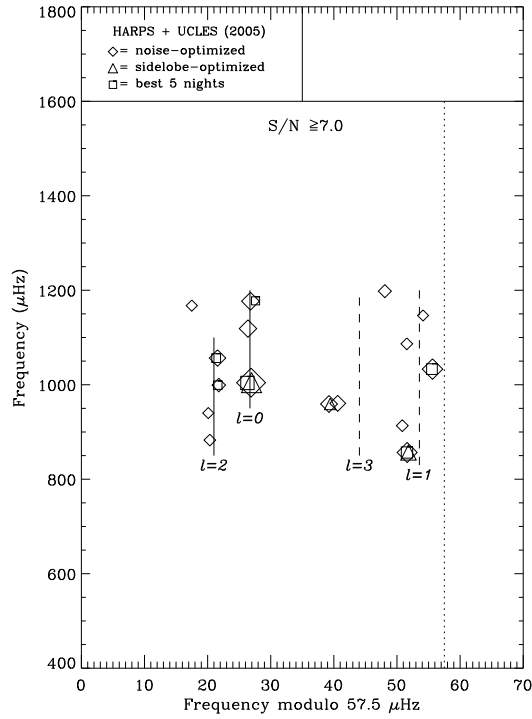


FIG. 8.— Échelle diagram of frequencies extracted from the 2005 observations. Only the strongest peaks are shown ($S/N \geq 7$). Different symbols identify the three weighting schemes (see § 2.1 and § 2.2) and the symbol size is proportional to the S/N . The solid lines mark our identification of $l = 0$ and $l = 2$, and these were used to calculate the positions for $l = 1$ and $l = 3$ (dashed lines), using the asymptotic relation (equation 2).

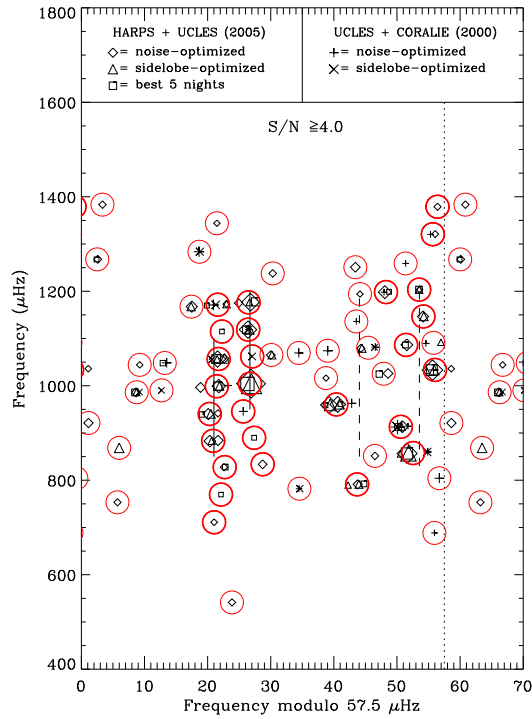


FIG. 9.— Same as Fig. 8 but also including the 2000 observations (see § 3) and with all peaks having $S/N \geq 4$. The red circles show the frequencies listed in Table 1, with thicker lines denoting modes for which we are confident of the identification.

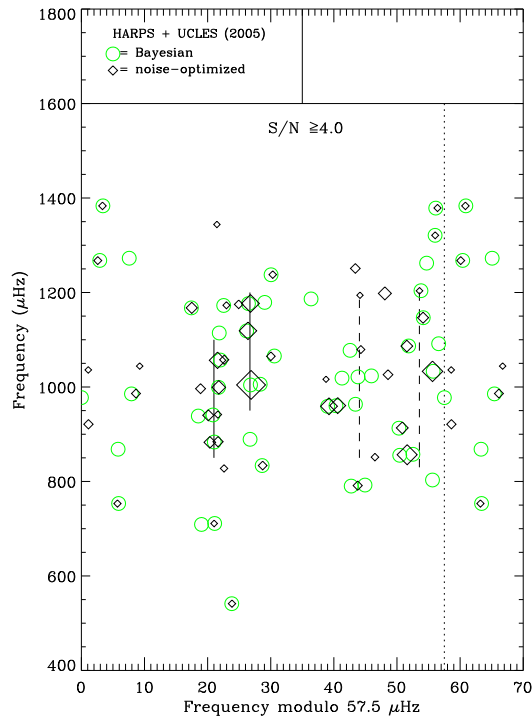


FIG. 10.— A comparison between frequencies present in the noise-optimized 2005 time series found using traditional iterative sine-wave fitting (diamonds; same as in Fig. 9) and the most probable peaks found using a Bayesian method (green circles; see § 4.1).

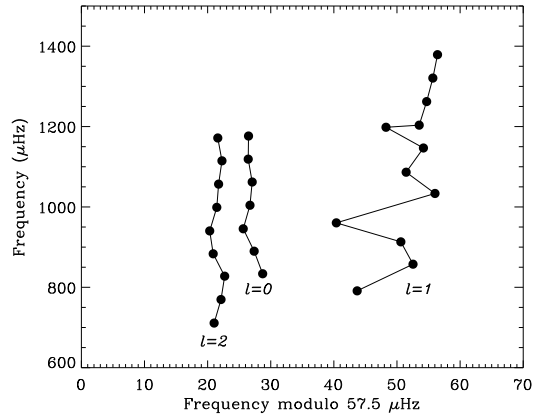


FIG. 11.— Échelle diagram of the 28 oscillation frequencies in β Hyi of which we are confident. The frequencies are given in the upper part of Table 1.

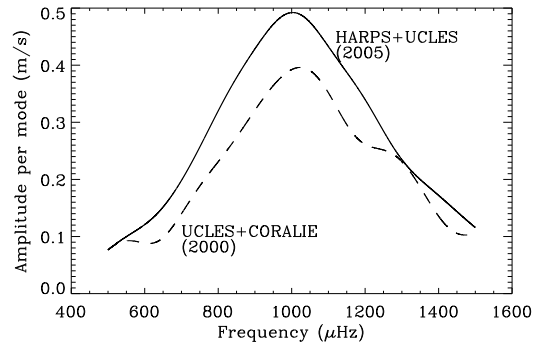


FIG. 12.— Amplitude of oscillations in β Hyi from the 2000 and 2005 observations (see § 5).

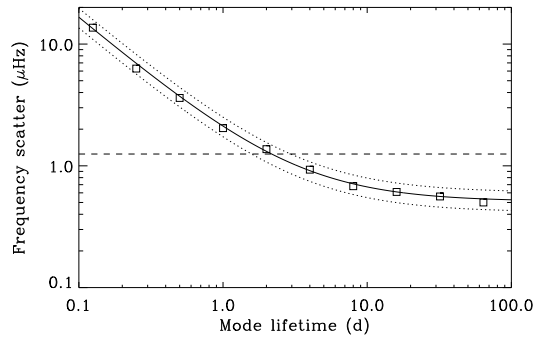


FIG. 13.— Calibration of the mode lifetime from measurements of the frequency scatter. Each point shows the mean of 300 simulations, each measuring the frequency scatter for a given mode lifetime. The solid curve is a fit to these points and the dotted curves show the $1-\sigma$ variations in the simulations. The horizontal dashed line shows the observed scatter in the frequencies, from which we can read off the mode lifetime of β Hyi (see § 6).

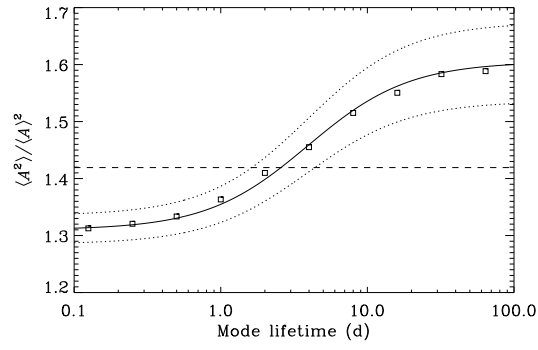


FIG. 14.— Calibration of the mode lifetime from measurements of the ratio of power-to-squared-amplitude in the noise-optimized power spectrum. Each point shows the mean of 300 simulations, each measuring the frequency scatter for a given mode lifetime. The solid curve is a fit to these points and the dotted curves show the $1\text{-}\sigma$ variations in the simulations. The horizontal dashed line shows the observed value of the ratio (see §6).

TABLE 1
OSCILLATION FREQUENCIES IN β HYI

ν (μHz)	$\nu \bmod \Delta\nu$ (μHz)	S/N	MODE ID
711.03 (1.49)	21.0	4.3	$l = 2, n = 10$
769.62 (1.59)	22.1	4.1	$l = 2, n = 11$
791.19 (1.06)	43.7	6.0	mixed
827.70 (1.19)	22.7	5.2	$l = 2, n = 12$
833.72 (1.10)	28.7	5.7	$l = 0, n = 13$
857.54 (0.86)	52.5	13.0	$l = 1, n = 13$
883.38 (0.94)	20.9	7.5	$l = 2, n = 13$
889.87 (1.45)	27.4	4.4	$l = 0, n = 14$
913.11 (0.89)	50.6	9.3	$l = 1, n = 14$
940.33 (0.95)	20.3	7.2	$l = 2, n = 14$
945.64 (1.13)	25.6	5.5	$l = 0, n = 15$
960.39 (0.87)	40.4	10.9	mixed
998.95 (0.90)	21.5	8.8	$l = 2, n = 15$
1004.21 (0.85)	26.7	18.8	$l = 0, n = 16$
1033.52 (0.86)	56.0	13.3	$l = 1, n = 16$
1056.74 (0.87)	21.7	10.7	$l = 2, n = 16$
1062.06 (1.27)	27.1	4.9	$l = 0, n = 17$
1086.45 (0.93)	51.4	7.6	$l = 1, n = 17$
1114.77 (1.49)	22.3	4.3	$l = 2, n = 17$
1118.93 (0.87)	26.4	11.3	$l = 0, n = 18$
1146.69 (0.95)	54.2	7.2	$l = 1, n = 18$
1171.61 (0.97)	21.6	7.0	$l = 2, n = 18$
1176.48 (0.87)	26.5	11.6	$l = 0, n = 19$
1198.26 (0.90)	48.3	8.5	mixed
1203.52 (1.04)	53.5	6.1	$l = 1, n = 19$
1262.20 (2.66)	54.7	3.0	$l = 1, n = 20$
1320.68 (1.40)	55.7	4.5	$l = 1, n = 21$
1378.92 (1.33)	56.4	4.7	$l = 1, n = 22$
541.36 (1.33)	23.9	4.7	
688.43 (1.59)	55.9	4.1	
753.22 (1.33)	5.7	4.7	
782.04 (1.37)	34.5	4.6	
804.21 (1.02)	56.7	6.3	
851.51 (1.27)	46.5	4.9	
868.49 (1.03)	6.0	6.2	
921.12 (1.04)	1.1	6.1	
986.27 (1.04)	8.8	6.1	
990.19 (1.59)	12.7	4.1	
1016.26 (1.59)	38.8	4.1	
1025.39 (1.02)	47.9	6.3	
1044.24 (1.54)	9.2	4.2	
1048.21 (1.03)	13.2	6.2	
1065.10 (1.11)	30.1	5.6	
1069.44 (1.07)	34.4	5.9	
1074.03 (1.02)	39.0	6.3	
1080.44 (1.17)	45.4	5.3	
1090.78 (1.45)	55.8	4.4	
1136.06 (1.65)	43.6	4.0	
1167.44 (0.95)	17.4	7.2	
1194.14 (1.59)	44.1	4.1	
1237.82 (1.27)	30.3	4.9	
1250.90 (1.02)	43.4	6.3	
1258.87 (1.49)	51.4	4.3	
1267.51 (1.22)	2.5	5.1	
1283.70 (0.99)	18.7	6.7	
1343.97 (1.54)	21.5	4.2	
1383.34 (1.27)	3.3	4.9	

TABLE 2
PARAMETERS FOR β HYI

Parameter	Value
$\Delta\nu_0$ at 1 mHz (μHz)	57.24 ± 0.16
$\Delta\nu_2$ at 1 mHz (μHz)	57.52 ± 0.10
$\delta\nu_{02}$ at 1 mHz (μHz)	5.32 ± 0.45
D_0 at 1 mHz (μHz)	0.89 ± 0.07
ϵ at 1 mHz	1.55 ± 0.05
$\bar{\rho}$ (g cm^{-3})	0.2538 ± 0.0015
mode lifetime (d)	$2.32^{+0.64}_{-0.51}$